Control of Grid-Connected Voltage-Source Converters

The Relationship between Direct-Power Control and Vector-Current Control

Gui, Yonghao; Wang, Xiongfei; Blåbjerg, Frede; Pan, Donghua

Published in:
I E E E Industrial Electronics Magazine

DOI (link to publication from Publisher):
10.1109/MIE.2019.2898012

Publication date:
2019

Document Version
Accepted author manuscript, peer reviewed version

Control of Grid-Connected Voltage-Source Converters: Relationship Between Direct Power Control and Vector Current Control

Yonghao Gui, *Member, IEEE*, Xiongfei Wang, *Senior Member, IEEE*, Frede Blaabjerg, *Fellow, IEEE*, and Donghua Pan, *Member, IEEE*.

Abstract

This article discusses the mathematical relationship between the grid-voltage-modulated-direct-power-control (GVM-DPC) and the vector-current-control (VCC) for three-phase voltage-source-converters (VSCs). It reveals that the GVM-DPC is equivalent to the VCC at the steady-state, yet presents a superior transient performance by removing the need of phase-locked loop (PLL). That means the GVM-DPC solves the disadvantage of conventional DPC such as poor steady-state performance. Moreover, the GVM-DPC will reduce the computational burden in comparison with the VCC due to the absence of Park transformation and PLL. Consequently, we can expect that the GVM-DPC method has a good capability of plug-and-play for the VSC. Finally, the experiment results match the theoretical expectations closely.

Index Terms

Direct power control, vector current control, voltage source converters, phase-locked loop.

I. Introduction of Control of Grid-Connected Voltage-Source Converters

Voltage source converter (VSC) is widely used in the application of smart grid, flexible AC transmission systems, and renewable energy sources (*e.g.,* wind and solar) [1]–[6]. Various control methods are researched for VSC to improve its performance, stability, and robustness [7].

Y. Gui was with the Department of Energy Technology, Aalborg University, and is now with Automation & Control section at the Department of Electronic Systems, Aalborg University, 9220 Aalborg, Denmark (e-mail: yg@es.aau.dk)

X. Wang, F. Blaabjerg, and D. Pan are with the Department of Energy Technology, Aalborg University, 9220 Aalborg, Denmark (e-mail: xwa@et.aau.dk; fbl@et.aau.dk; dop@et.aau.dk).

The conventional control of grid-connected VSC is using vector current controller (VCC), which is designed in a synchronously rotating reference frame and a proportional integral (PI) control with a decoupling term is applied to control *d*–*q* axes currents independently [8]. The key point is that it uses coordinate transformation to transform the AC components to the DC ones and thus the linear PI controller can be used. Moreover, the VSC system is changed to a linear time invariant (LTI) system in the rotating reference frame, which means that the system can be readily designed and analyzed through linear control techniques [9]–[11]. The main disadvantage of the conventional VCC is that it suffers from a slow transient response, since it uses a phase-locked loop (PLL) system for the coordinate transformation. In addition, the interaction between the PLL system and the current loop control system causes harmonic problem in a weak grid, even destabilizes the system [12]–[15].

An alternative control strategy has emerged for induction machine drives, which is the direct torque control (DTC) [16], [17]. It has a simple structure in comparison with the VCC. To achieve the constant switching frequency, a modified DTC strategy based on space vector modulation was developed [18], [19]. Based on the DTC strategy concept, the direct power control (DPC) was developed for grid-connected VSCs [20]–[22]. In [20] and [21], a look-up-table (LUT)-DPC was developed, where the proper switching states are selected from a predefined optimal switching table based on the instantaneous errors of active and reactive powers and the angular position of the VSC terminal voltage. However, the variable switching frequency is resulted with a broadband harmonic spectra, which complicates the design of line filters. To solve such a problem, various DPC algorithms were developed for a constant switching frequency [23], [24]. In addition, for a robust control, the sliding mode control (SMC) based DPC [25] and passivity-based control (PBC)-DPC [26] have been reported to obtain a faster transient response than that of the PI controller and a better robustness to parameter uncertainties than that of the LUT-DPC. However, there are still large ripples in both active and reactive powers. Another control strategy, i.e. model predictive control (MPC)-DPC performs a good closed loop behavior with consideration of the system constraints [27], [28]. However, an incorrect voltage sequence selection could affect its performance [29]. Recently, a grid voltage modulated-DPC (GVM-DPC) was introduced in [30] to design a robust but simple control law for not only the convergence rate of the instantaneous active and reactive powers, but also the steady-state performance of VSC, especially reducing the power ripples and total harmonics distortion (THD) of the output current in comparison with the SMC-DPC and PBC-DPC. Another advantage of the GVM-DPC

is that it converts the original nonlinear system into an LTI one, which can easily be analyzed and designed by using the conventional linear control techniques [31]. In [32], Gui *et al.* proposed a novel vector current control method based on the concept of the GVM-DPC.

Although the GVM-DPC shows a better steady-state performance compared with the SMC-DPC and PBC-DPC, there is no analysis to explain how and why it can obtain a better performance in detail. This article is firstly to present a main feature between the GVM-DPC and the conventional VCC designed in d-q frame for three-phase VSC in detail. We mathematically prove that the DPC model of VSC is equal to the current model in the d-q frame, which reveals that the GVM-DPC is equivalent to the VCC at the steady state, yet presents superior transient performance by removing the need of the PLL. That means, the GVM-DPC method could achieve the same property of steady-state performance as the VCC but better tracking performance, since there is no PLL. In addition, the GVM-DPC method will reduce computational burden in comparison with the VCC since there is no Park transformation or a PLL system. Consequently, it can be expected that the GVM-DPC method could be applied to various applications and be modified to solve various industry issues.

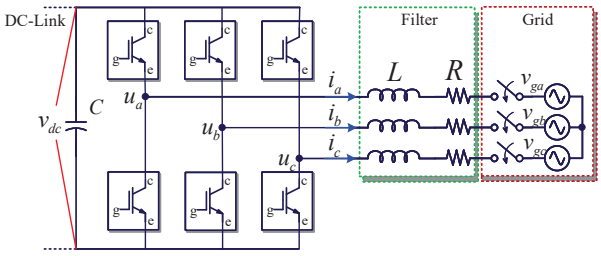

Fig. 1. Grid connected two level voltage source converter with an L filter.

II. Grid Voltage Modulated Direct Power Control

In this section, firstly, a model of the VSC in the stationary reference frame is described. Then, the DPC modeling of VSC is briefly introduced. For the VSC system, the GVM-DPC is designed to make it be an LTI multi-input-multi-output (MIMO) system.

A. Modeling of vector current control

Fig. 1 shows a simplified circuit of a two-level VSC connected to the grid with an L-filter. The DC side could be connected to renewable energy sources or energy storage systems with a

capacitor C. The relationship among the VSC output voltages, the grid voltages, and the output currents can be expressed as follows:

$$\begin{aligned} u_a &= Ri_a + L\frac{di_a}{dt} + v_{ga}, \\ u_b &= Ri_b + L\frac{di_b}{dt} + v_{gb}, \\ u_c &= Ri_c + L\frac{di_c}{dt} + v_{gc}, \end{aligned} \tag{1}$$

where $v_{ga,b,c}$, i_{abc}, and u_{abc} are the three-phase of grid voltage, input current, and VSC voltage, respectively. L and R are the filter inductance and resistance, respectively. The Clark transformation is defined as follows [33]:

$$T_{abc2\alpha\beta} = \frac{2}{3}\begin{bmatrix} 1 & -\frac{1}{2} & -\frac{1}{2} \\ 0 & -\frac{\sqrt{3}}{2} & -\frac{\sqrt{3}}{2} \end{bmatrix}. \tag{2}$$

Based on a balanced grid voltage condition, the relationship in (1) can be expressed in the stationary reference frame by using Clark transformation in (2) as [34]

$$\begin{aligned} u_\alpha &= Ri_\alpha + L\frac{di_\alpha}{dt} + v_{g\alpha}, \\ u_\beta &= Ri_\beta + L\frac{di_\beta}{dt} + v_{g\beta}, \end{aligned} \tag{3}$$

where $v_{g\alpha}$ and $v_{g\beta}$ indicate the grid voltages, i_α and i_β indicate the output currents, and u_α and u_β indicate the VSC output voltages in the alpha-beta frame. Then, we give Park transformation.

$$T_{\alpha\beta 2dq} = \begin{bmatrix} cos(\theta) & sin(\theta) \\ -sin(\theta) & cos(\theta) \end{bmatrix}, \tag{4}$$

where θ is a phase angle and usually calculated by using PLL. In this study, the d-axis is always coincident with the instantaneous voltage vector and the q-axis is in quadrature with it, i.e., $v_{gd} = V_g$ and $v_{gq} = 0$. By using Park transformation in (4), the current model (3) can be presented in the d-q frame as [33]

$$\begin{aligned} L\frac{di_d}{dt} &= -Ri_d + L\omega i_q + u_d - v_{gd}, \\ L\frac{di_q}{dt} &= -L\omega i_d - Ri_q + u_q, \end{aligned} \tag{5}$$

where v_{gd} and v_{gq} indicate the grid voltages, i_d and i_q indicate the output currents, and u_d and u_q indicate the VSC output voltages in d-q frame. ω is the angular frequency of the grid voltage and $\omega = 2\pi f$, and f is the frequency of the grid voltage.

B. Modeling of DPC

We define the instantaneous active and reactive powers of the VSC in the stationary reference frame as follows [34]:

$$\begin{aligned} P &= \frac{3}{2}(v_{g\alpha} i_\alpha + v_{g\beta} i_\beta), \\ Q &= \frac{3}{2}(v_{g\beta} i_\alpha - v_{g\alpha} i_\beta), \end{aligned} \tag{6}$$

where P and Q are the active and reactive powers of the VSC, respectively. We can express the instantaneous active and reactive powers variation based on the grid voltages and output currents variation by differentiating (6) as follows:

$$\begin{aligned} \frac{dP}{dt} &= \frac{3}{2}\left(i_\alpha \frac{dv_{g\alpha}}{dt} + v_{g\alpha}\frac{di_\alpha}{dt} + i_\beta \frac{dv_{g\beta}}{dt} + v_{g\beta}\frac{di_\beta}{dt}\right), \\ \frac{dQ}{dt} &= \frac{3}{2}\left(i_\alpha \frac{dv_{g\beta}}{dt} + v_{g\beta}\frac{di_\alpha}{dt} - i_\beta \frac{dv_{g\alpha}}{dt} - v_{g\alpha}\frac{di_\beta}{dt}\right). \end{aligned} \tag{7}$$

In this study, we consider a non-distorted grid. Thus, we can obtain the following relationship such as

$$\begin{aligned} v_{g\alpha} &= V_g \cos(\omega t), \\ v_{g\beta} &= V_g \sin(\omega t), \end{aligned} \tag{8}$$

where V_g is the amplitude of the grid voltage. Then, the instantaneous grid voltage variations can be obtained by differentiating (8) as follows:

$$\begin{aligned} \frac{dv_{g\alpha}}{dt} &= -\omega V_g \sin(\omega t) = -\omega v_{g\beta}, \\ \frac{dv_{g\beta}}{dt} &= \omega V_g \cos(\omega t) = \omega v_{g\alpha}. \end{aligned} \tag{9}$$

Substituting (3) and (9) into (7), we can obtain a state-space model of the active and reactive powers as follows:

$$\begin{aligned} \frac{dP}{dt} &= -\frac{R}{L}P - \omega Q + \frac{3}{2L}(v_{g\alpha}u_\alpha + v_{g\beta}u_\beta - V_g^2), \\ \frac{dQ}{dt} &= \omega P - \frac{R}{L}Q + \frac{3}{2L}(v_{g\beta}u_\alpha - v_{g\alpha}u_\beta). \end{aligned} \tag{10}$$

C. Grid voltage modulated direct power control

As represented in (10), the dynamics of VSC with an L fiter is a time-varying MIMO system. In [30], the GVM control inputs are defined to decouple the outputs from the two inputs as follows:

$$\begin{bmatrix} u_P \\ u_Q \end{bmatrix} = \begin{bmatrix} v_{g\alpha}u_\alpha + v_{g\beta}u_\beta \\ -v_{g\beta}u_\alpha + v_{g\alpha}u_\beta \end{bmatrix}. \tag{11}$$

Based on (8), the new GVM control inputs (11) are possible to be represented in the d-q frame as follows:

$$\begin{bmatrix} u_P \\ u_Q \end{bmatrix} = V_g \underbrace{\begin{bmatrix} \cos(\omega t) & \sin(\omega t) \\ -\sin(\omega t) & \cos(\omega t) \end{bmatrix}}_{Park\ Transformation} \begin{bmatrix} u_\alpha \\ u_\beta \end{bmatrix} = V_g \begin{bmatrix} u_d \\ u_q \end{bmatrix}, \tag{12}$$

Based on (12), the original system (10) can be represented as follows:

$$\begin{aligned} \frac{dP}{dt} &= -\frac{R}{L}P - \omega Q + \frac{3}{2L}(u_P - V_g^2), \\ \frac{dQ}{dt} &= \omega P - \frac{R}{L}Q - \frac{3}{2L}u_Q. \end{aligned} \tag{13}$$

The GVM-DPC presents the system in the d–q frame without using the PLL. Notice that, (13) is converted into an LTI system with some coupling states. Consequently, it can be easily analyzed and designed by using conventional linear control techniques [31].

III. Relationship Between DPC and VCC

In this section, we show a relationship between the GVM-DPC and the conventional VCC designed in synchronous rotating frame. Then, the conventional VCC and the GVM-DPC methods are designed and compared.

A. Relationship between GVM-DPC and VCC

Since the system in (5) is defined where the d-axis is always coincident with the instantaneous voltage vector and the q-axis is in quadrature with it, $v_{gd} = V_g$ and $v_{gq} = 0$. Consequently. the active and reactive powers in the d-q frame can be defined as follows:

$$\begin{aligned} P &= \frac{3}{2}V_g i_d, \\ Q &= -\frac{3}{2}V_g i_q. \end{aligned} \tag{14}$$

If we multiply $\frac{2}{3V_g}$ to both side of (13), then a new system can be obtained as follows:

$$\begin{aligned} \frac{di_d}{dt} &= -\frac{R}{L}i_d + \omega i_q + \frac{1}{L}(u_d - V_g), \\ \frac{di_q}{dt} &= -\omega i_d - \frac{R}{L}i_q + \frac{1}{L}u_q. \end{aligned} \tag{15}$$

It is obvious that the DPC model is changed into a conventional d-q currents model. Consequently, we can achieve zero steady-state error by using a PI controller which is the same as the VCC. In contrast, we can expect that the controller designed based on (13) will obtain a faster transient response because there is no need for PLL.

B. Vector current control designed in d-q frame

In this article, we only show a traditional controller consisting of feedforward and feedback to regulate d-q axes currents. At first, we define errors of d-q axes currents as follows:

$$\begin{aligned} e_{i_d} &:= i_{dref} - i_d, \\ e_{i_q} &:= i_{qref} - i_q, \end{aligned} \tag{16}$$

where i_{dref} and i_{qref} are d-q axes currents references, respectively. A controller consisting of feedforward and feedback is designed as follows [35]:

$$\begin{aligned} u_d &= \underbrace{V_g - L\omega i_q}_{feedforward} + \underbrace{L\nu_{i_d}}_{feedback}, \\ u_q &= \underbrace{L\omega i_d}_{feedforward} + \underbrace{L\nu_{i_q}}_{feedback}, \end{aligned} \tag{17}$$

where ν_{i_d} and ν_{i_q} are the feedback control inputs. To obtain zero steady-state error, a PI controller is applied to ν_{i_d} and ν_{i_q} as follows:

$$\begin{aligned} \nu_{i_d} &= K_{i_d,p} e_{i_d} + K_{i_d,i} \int_0^t e_{i_d}(\tau) d\tau, \\ \nu_{i_q} &= K_{i_q,p} e_{i_q} + K_{i_q,i} \int_0^t e_{i_q}(\tau) d\tau, \end{aligned} \tag{18}$$

where $K_{i_d,p}$, $K_{i_d,i}$, $K_{i_q,p}$, and $K_{i_q,i}$ are the PI controller gains. For the PI controller gain design, substituting from (16) to (18) into (15), the closed-loop system can be obtained such as

$$\begin{aligned} \frac{di_d}{dt} &= -\frac{R}{L} i_d + K_{i_d,p}(i_{dref} - i_d) + K_{i_d,i} \int (i_{dref} - i_d) dt, \\ \frac{di_q}{dt} &= -\frac{R}{L} i_1 + K_{i_q,p}(i_{qref} - i_q) + K_{i_q,i} \int (i_{qref} - i_q) dt. \end{aligned} \tag{19}$$

If we differentiate (19), then it is changed to a second-order system as

$$\begin{aligned} \frac{d^2 i_d}{dt^2} &= -\frac{R}{L}\frac{di_d}{dt} + K_{i_d,p}\frac{d(i_{dref} - i_d)}{dt} + K_{i_d,i}(i_{dref} - i_d), \\ \frac{d^2 i_q}{dt^2} &= -\frac{R}{L}\frac{di_q}{dt} + K_{i_q,p}\frac{d(i_{qref} - i_q)}{dt} + K_{i_q,i}(i_{qref} - i_q). \end{aligned} \tag{20}$$

Applying the Laplace transform to (20) yields

$$\begin{aligned} s^2 i_d &= -\frac{R}{L} s i_d + K_{i_d,p} s(i_{dref} - i_d) + K_{i_d,i}(i_{dref} - i_d), \\ s^2 i_q &= -\frac{R}{L} s i_q + K_{i_q,p} s(i_{qref} - i_q) + K_{i_q,i}(i_{qref} - i_q) \end{aligned} \tag{21}$$

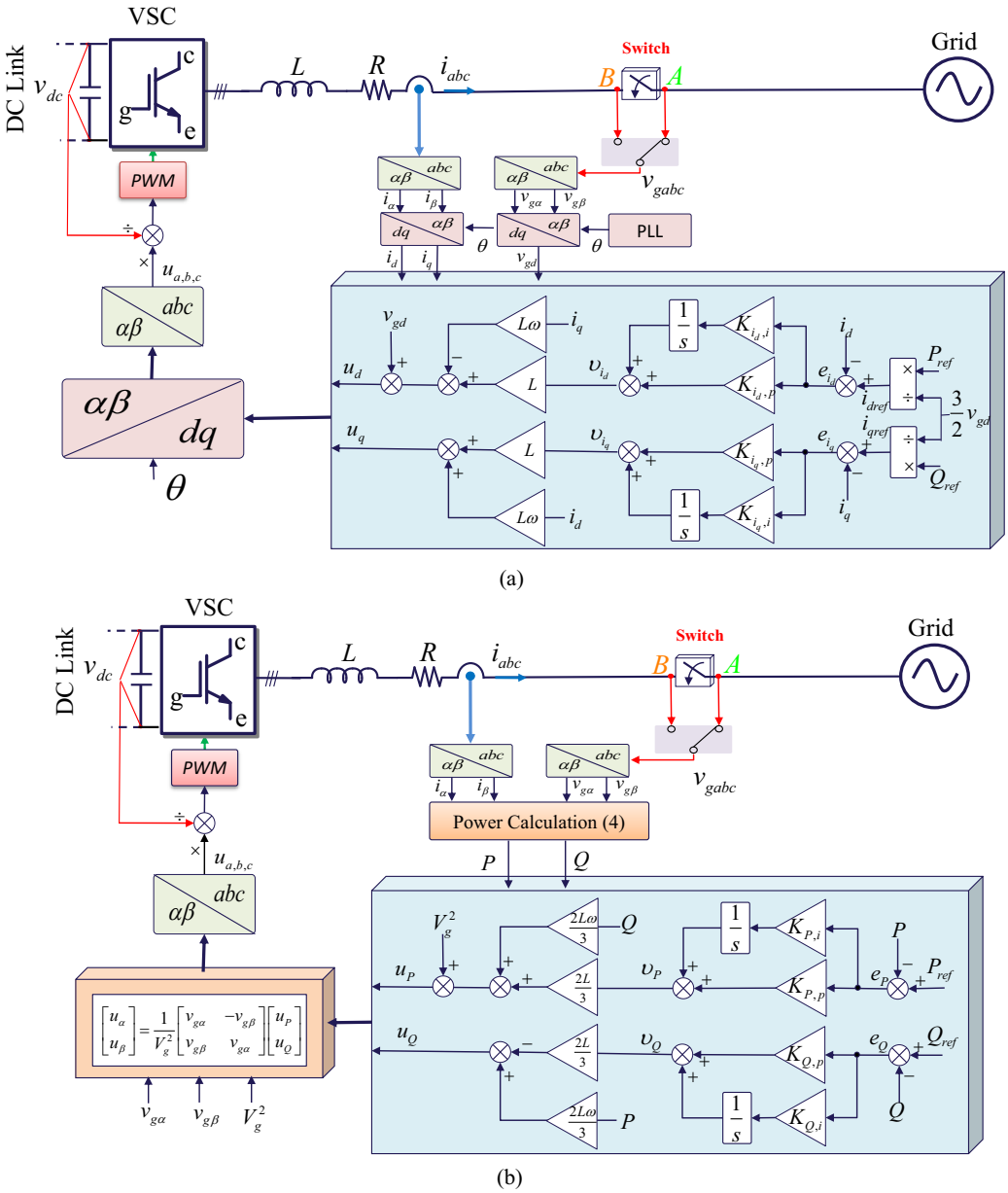

Fig. 2. Block diagram of (a) conventional vector current controller, (b) grid voltage modulated direct power control.

or equivalently

$$\begin{aligned} \frac{i_d(s)}{i_{dref}(s)} &= \frac{K_{i_d,p}s + K_{i_d,i}}{s^2 + (K_{i_d,p} + \frac{R}{L})s + K_{i_d,i}}, \\ \frac{i_q(s)}{i_{qref}(s)} &= \frac{K_{i_q,p}s + K_{i_q,i}}{s^2 + (K_{i_q,p} + \frac{R}{L})s + K_{i_q,i}}. \end{aligned} \tag{22}$$

The PI controller gains could be selected based on the traditional second-order system (22) [36].

C. Controller design for GVM-DPC

In this Subsection, a conventional controller including feedforward and feedback is designed to make the active and reactive powers track their references. Define errors of the active and reactive powers as follows:

$$\begin{aligned} e_P &:= P_{ref} - P, \\ e_Q &:= Q_{ref} - Q, \end{aligned} \tag{23}$$

where P_{ref} and Q_{ref} are the active and reactive power references, respectively. To compare with the conventional VCC fairly, we design the same control structure as the one designed in the d-q frame. To cancel the coupling terms. we take a control law with a feedforward and feedback such as

$$\begin{aligned} u_P &= \underbrace{V_g^2 + \frac{2L\omega}{3}Q}_{feedforward} + \underbrace{\frac{2L}{3}\nu_P}_{feedback}, \\ u_Q &= \underbrace{\frac{2L\omega}{3}P}_{feedforward} - \underbrace{\frac{2L}{3}\nu_Q}_{feedback}, \end{aligned} \tag{24}$$

where ν_P and ν_Q are the feedback control inputs. To obtain zero steady-state error, PI controller is applied to ν_P and ν_Q as follows:

$$\begin{aligned} \nu_P &= K_{P,p}e_P + K_{P,i}\int_0^t e_P(\tau)d\tau, \\ \nu_Q &= K_{Q,p}e_Q + K_{Q,i}\int_0^t e_Q(\tau)d\tau, \end{aligned} \tag{25}$$

where $K_{P,p}$, $K_{P,i}$, $K_{Q,p}$, and $K_{Q,i}$ are the PI controller gains. Finally, the original control inputs can be calculated based on the inverse of (11).

Notice that, if we use controller gains as positive values, the system is globally exponentially stable [37]. For the controller gain design, substituting from (23) to (25) into (13), the closed-loop system is obtained such as

$$\begin{aligned} \frac{dP}{dt} &= -\frac{R}{L}P + K_{P,p}(P_{ref} - P) + K_{P,i}\int (P_{ref} - P)dt, \\ \frac{dQ}{dt} &= -\frac{R}{L}Q + K_{Q,p}(Q_{ref} - Q) + K_{Q,i}\int (Q_{ref} - Q)dt. \end{aligned} \tag{26}$$

If we differentiate (26), then it is changed to a second-order system as

$$\begin{aligned} \frac{d^2P}{dt^2} &= -\frac{R}{L}\frac{dP}{dt} + K_{P,p}\frac{d(P_{ref} - P)}{dt} + K_{P,i}(P_{ref} - P), \\ \frac{d^2Q}{dt^2} &= -\frac{R}{L}\frac{dQ}{dt} + K_{Q,p}\frac{d(Q_{ref} - Q)}{dt} + K_{Q,i}(Q_{ref} - Q). \end{aligned} \tag{27}$$

Applying the Laplace transform to (27) yields

$$\begin{aligned} s^2P &= -\frac{R}{L}sP + K_{P,p}s(P_{ref} - P) + K_{P,i}(P_{ref} - P), \\ s^2Q &= -\frac{R}{L}sQ + K_{Q,p}s(Q_{ref} - Q) + K_{Q,i}(Q_{ref} - Q) \end{aligned} \tag{28}$$

or equivalently

$$\begin{aligned} \frac{P(s)}{P_{ref}(s)} &= \frac{K_{P,p}s + K_{P,i}}{s^2 + (K_{P,p} + \frac{R}{L})s + K_{P,i}}, \\ \frac{Q(s)}{Q_{ref}(s)} &= \frac{K_{Q,p}s + K_{Q,i}}{s^2 + (K_{Q,p} + \frac{R}{L})s + K_{Q,i}}. \end{aligned} \tag{29}$$

Fig. 2(b) shows the block diagram of the GVM-DPC method. Notice that both the VCC and the GVM-DPC methods consist of a similar structure with the feedforward and PI feedback. To compare with the VCC, the GVM-DPC method has only power calculation (6) and original input calculation. However, the VCC includes PLL, Park transformation, and inverse Park transformation. Consequently, we can conclude that the GVM-DPC method reduces the computational burden.

D. Controller gains tuning

Normally, the PI controller gains of the VCC method are tuned considering the overall system dynamics, which are evaluated by the crossover frequency ω_c and the phase margin (PM). With the consideration of the time delay, which consists of one sampling period (T_s) of computation delay and half sampling period ($0.5T_s$) of pulse-width modulation (PWM) delay [38], ω_c is related to PM by [39]

$$\omega_c = \frac{\pi/2 - \text{PM}}{1.5T_s}. \tag{30}$$

Based on ω_c in (30), the proportional gain K_p can be obtained approximately as

$$K_p \approx \omega_c L. \tag{31}$$

To minimize the phase contribution of the PI regulator at ω_c, its corner frequency is usually set a decade below ω_c [40]. Thus, the integral gain K_i can be calculated as

$$K_i = \frac{\omega_c}{10}K_p. \tag{32}$$

Since the GVM-DPC gets the same closed-loop dynamics as the VCC method, its controller gains can also be calculated based on the aforementioned procedure.

TABLE I

SYSTEM PARAMETERS USED IN SIMULATION

Parameter	Value
Nominal bus voltage, V_{rms}	110 V
Nominal bus frequency, f	50 Hz
Filter inductance, L	5 mH
Filter resistance, R	0.2 Ω
Switching frequency, f_{sw}	10 kHz
Sampling period, T_s	0.1 ms

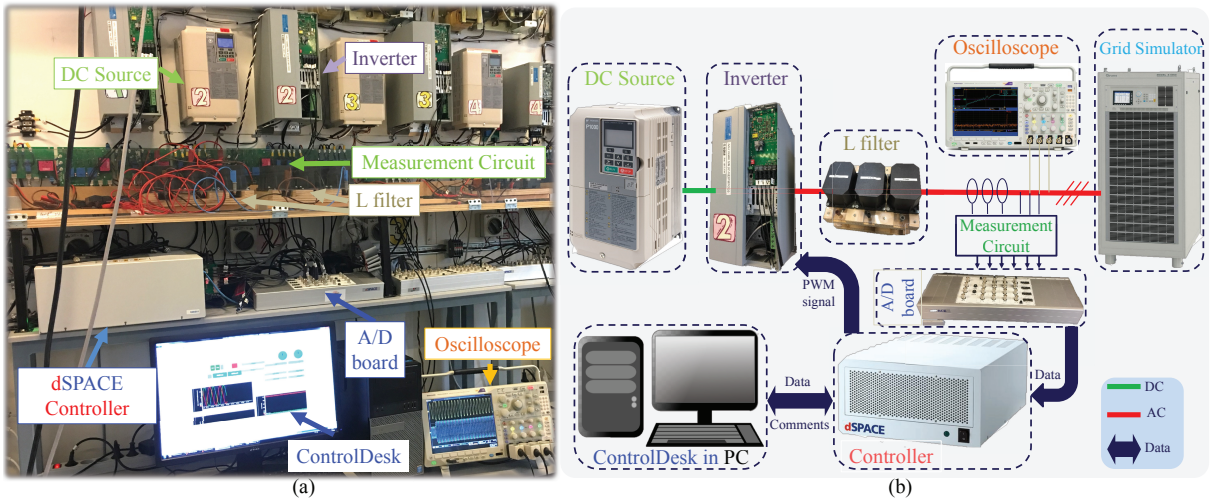

Fig. 3. (a) Experimental test setup in the laboratory at Aalborg University; (b) Configuration of the setup.

IV. PERFORMANCE VALIDATION

The effectiveness of the GVM-DPC method is compared with the VCC by using a three-leg three-phase 15-kVA inverter with an L filter. The control system is implemented by using the DS1007 dSPACE system, where the switching pulses are generated by using the DS5101 digital waveform output board, and the grid voltages and currents are measured by using the DS2004 high-speed A/D board. A constant dc voltage supply is used at the dc-side. Furthermore, the ac-side is connected to a grid simulator, which generates 110 V, as shown in Fig. 3. The parameters of the system used in the experimental test are listed in Table I. In the test, the PM in (30) is set to $45°$.

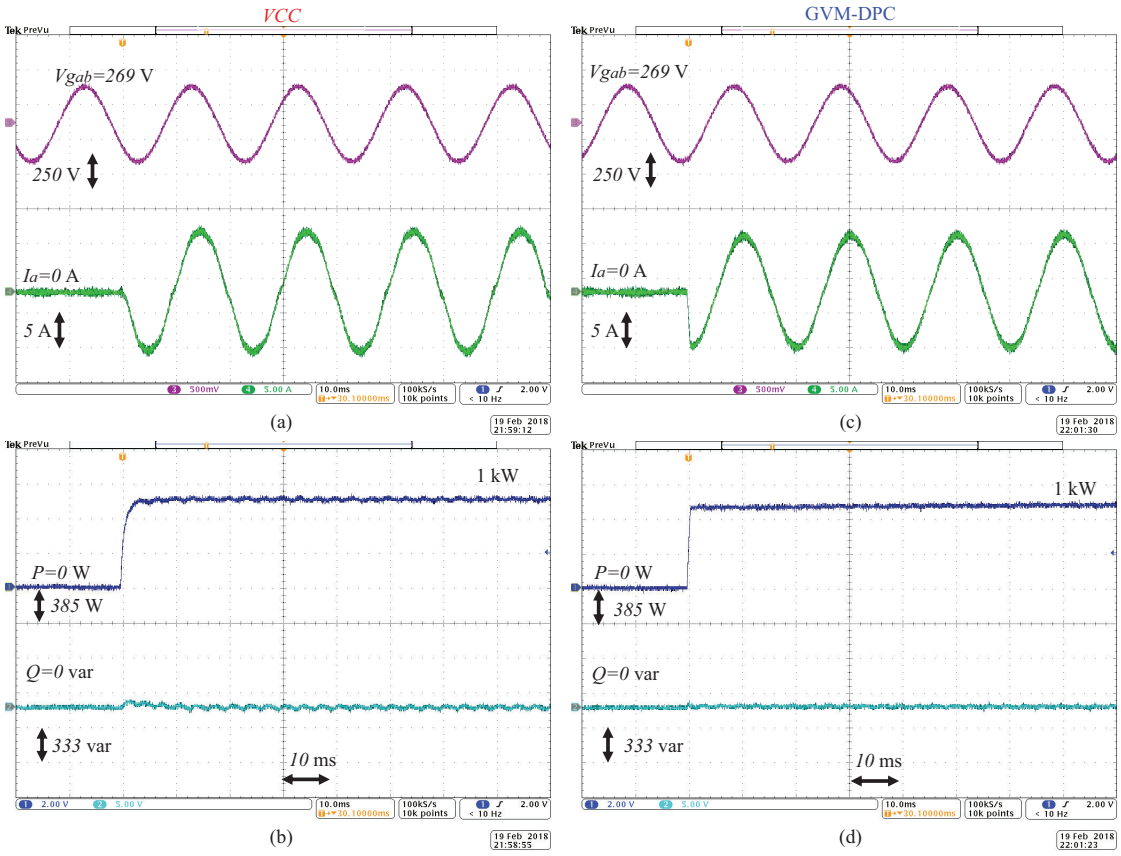

Fig. 4. Experimental results when the active power step changes. Vector current control: (a) line-to-line grid voltage (V_{gab}) and current (I_a); (b) active and reactive powers. Grid voltage modulated direct power control: (c) line-to-line grid voltage (V_{gab}) and current (I_a); (d) active and reactive powers.

As the first test, the reference of the active power is changed from 0 kW to 1 kW. Fig. 4 shows the time response of the VCC and the GVM-DPC methods. In this case, it should be noted that the grid voltages are measured at 'A' point in Fig. 2 (*i.e.,* the VSC continuously measures the grid voltages even it is not injecting powers, as shown in Fig. 4). The main disadvantage of the conventional DPC method is the steady-state performance (*i.e.,* power ripple) compared to the VCC method designed in the *d-q* frame [25], [37]. However, the GVM-DPC has a similar active power tracking performance compared to the VCC method, as shown in Fig. 4. Moreover, from Fig. 5, the THDs of the output current using both methods are similar, since the GVM-DPC method has a same model as that in d-q frame, as we discussed in Section II. In this case, the PLL system can continually provide the correct information of phase angle, hence, we can conclude that the results in Fig. 4 are acceptable.

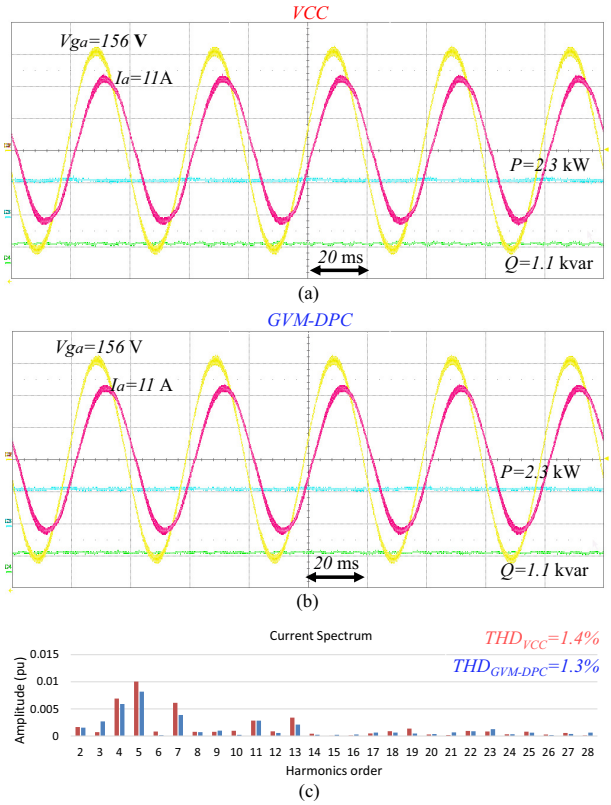

Fig. 5. Measured performance of (a) vector current controller and (b) grid voltage modulated direct power control when $P = 2.3$ kW and $Q = 1.1$ kvar. (c) Spectrum analysis of current. (Yellow line: grid voltage V_{ga}, pink-red line: output current I_a, sky-blue line: P, and Green line: Q.)

In addition, we test the robustness of the both methods to the grid voltage, *i.e.* low voltage ride through (LVRT) capability. Fig. 6 shows the time response of the VCC and GVM-DPC methods when the grid has a 100% balanced voltage sag. In this case, we set the references as $P_{ref} = 0.5$ kW and $Q_{ref} = 0$ kVar, and $P_{ref} = 0$ kW at the time when the fault happens. It can be observed that the line current with the VCC has a large overshoot at the time when the voltage sag happens. Especially, when the grid voltage returns to its nominal value after faults, the active power with the VCC method has a larger overshoot compared to the GVM-DPC one, since the slow dynamics of the PLL system. However, the trajectory with the GVM-DPC method converges to its new operating point fast, even at the time when the fault clears. The case, where the grid voltages are measured from 0 to its nominal value, can also be found in the module uninterruptible power supply (UPS) system, which has a hot-swap operation property [41]. That means when one UPS module fails, the redundant power modules have to take over immediately

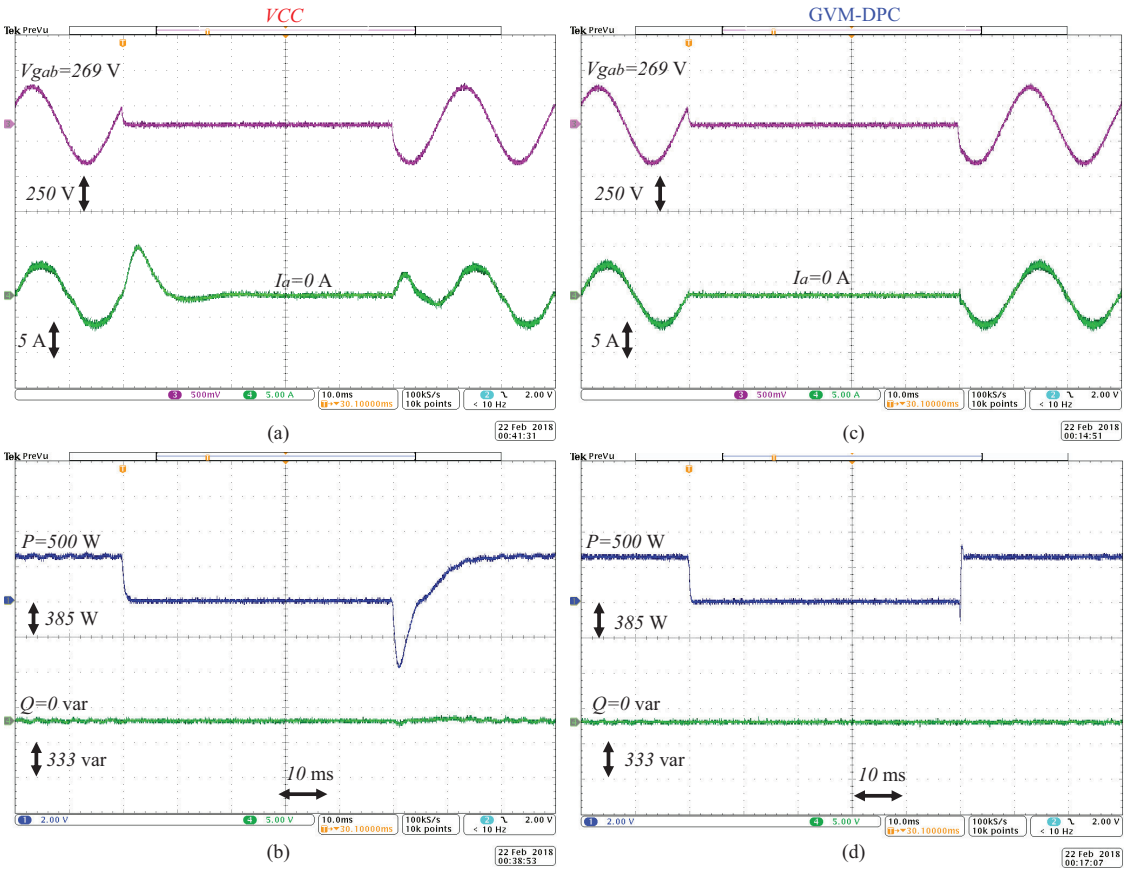

Fig. 6. LVRT performance when the grid has 100% voltage sag. Vector current control: (a) line-to-line grid voltage (V_{gab}) and current (I_a); (b) active and reactive powers. Grid voltage modulated direct power control: (c) line-to-line grid voltage (V_{gab}) and current (I_a); (d) active and reactive powers.

to guarantee the electricity supply to the loads. Hence, the redundant power modules do nothing in normal time, (*i.e.*, the grid voltages are not measured at 'B' point in Fig. 2). It can be expected that the GVM-DPC has an enhanced capability of the plug-and-play.

Finally, we test the both methods in a weak grid, where the frequency and the phase shift step and fluctuate [42]. In this case, we use 22 mH–L and 15 μF–C to construct a grid impedance, where the short circuit ratio is 1.5. From Fig. 7(a), it is observed that the VCC method destabilizes the system due to the PLL system as discussed in [15]. However, the GVM-DPC method can stabilize the system since it eliminates the PLL system, as shown in Fig. 7(b). Consequently, we can conclude that the GVM-DPC has same property in the normal cases but it has good dynamic capabilities in some special cases, where the PLL system makes some problem.

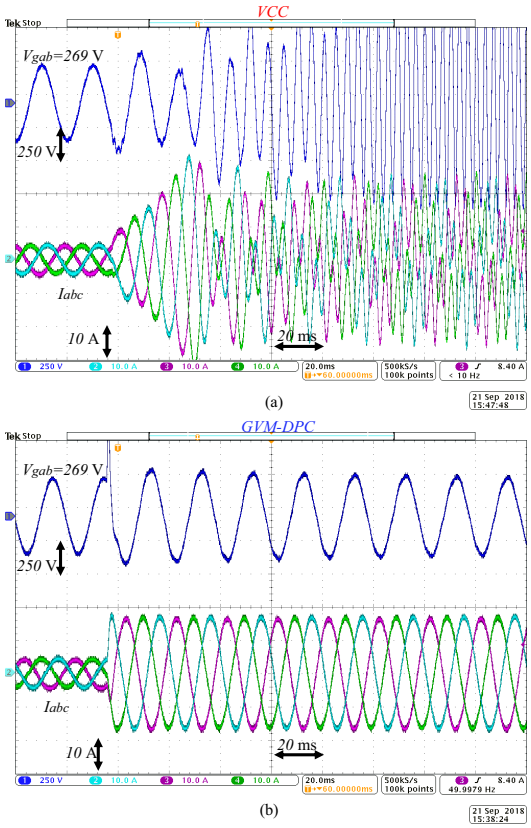

Fig. 7. Measured time response of the VSC when the active power is injected to the grid from 0.5 kW to 2 kW. (a) Vector current control; (b) grid voltage modulated direct power control.

V. Conclusions

In this article, we presented a relationship between GVM-DPC and the VCC designed in synchronous rotating reference frame for three-phase VSC. We mathematically showed that the GVM-DPC is equal to the current model in the synchronous rotating reference frame. That means the GVM-DPC could achieve the same steady-state performance as the VCC but better tracking performance because of PLL elimination in the control method implementation. Furthermore, the GVM-DPC will reduce the computational burden in comparison with the synchronous controller since there is neither d-q transformation nor PLL system. Finally, the experimental results show that the GVM-DPC has same property in the normal cases as the VCC but it has better dynamic capabilities in some special cases, where the PLL system makes the problem.

In the future, the GVM-DPC will be modified for various applications to overcome their practical issues.

REFERENCES

[1] M. Liserre, T. Sauter, and J. Y. Hung, "Future energy systems: Integrating renewable energy sources into the smart power grid through industrial electronics," *IEEE Ind. Electron. Mag.*, vol. 4, no. 1, pp. 18–37, 2010.

[2] F. Blaabjerg, M. Liserre, and K. Ma, "Power electronics converters for wind turbine systems," *IEEE Trans. Ind. Appl.*, vol. 48, no. 2, pp. 708–719, 2012.

[3] S. Kouro, J. I. Leon, D. Vinnikov, and L. G. Franquelo, "Grid-connected photovoltaic systems: An overview of recent research and emerging PV converter technology," *IEEE Ind. Electron. Mag.*, vol. 9, no. 1, pp. 47–61, 2015.

[4] Y. Gui, W. Kim, and C. C. Chung, "Passivity-based control with nonlinear damping for type 2 STATCOM systems," *IEEE Trans. Power Syst.*, vol. 31, no. 4, pp. 2824–2833, 2016.

[5] F. Blaabjerg, Y. Yang, D. Yang, and X. Wang, "Distributed power-generation systems and protection," *Proc. IEEE*, vol. 105, no. 7, pp. 1311–1331, 2017.

[6] X. Guo, B. Wei, T. Zhu, Z. Lu, L. Tan, X. Sun, and C. Zhang, "Leakage current suppression of three-phase flying capacitor PV inverter with new carrier modulation and logic function," *IEEE Trans. Power Electron.*, vol. 33, no. 3, pp. 2127–2135, 2018.

[7] X. Wang, F. Blaabjerg, M. Liserre, Z. Chen, J. He, and Y. Li, "An active damper for stabilizing power-electronics-based AC systems," *IEEE Trans. Power Electron.*, vol. 29, no. 7, pp. 3318–3329, 2014.

[8] M. Kazmierkowski and L. Malesani, "Current control techniques for three-phase voltage-source PWM converters: a survey," *IEEE Trans. Ind. Electron.*, vol. 45, no. 5, pp. 691–703, Oct. 1998.

[9] M. Reyes, P. Rodriguez, S. Vazquez, A. Luna, R. Teodorescu, and J. M. Carrasco, "Enhanced decoupled double synchronous reference frame current controller for unbalanced grid-voltage conditions," *IEEE Trans. Power Electron.*, vol. 27, no. 9, pp. 3934–3943, 2012.

[10] Z. Li, C. Zang, P. Zeng, H. Yu, S. Li, and J. Bian, "Control of a grid-forming inverter based on sliding-mode and mixed H_2/H_∞ control," *IEEE Trans. Ind. Electron.*, vol. 64, no. 5, pp. 3862–3872, 2017.

[11] X. Wang, L. Harnefors, and F. Blaabjerg, "Unified impedance model of grid-connected voltage-source converters," *IEEE Trans. Power Electron.*, vol. 33, no. 2, pp. 1775–1787, 2018.

[12] P. Rodríguez, A. Luna, I. Candela, R. Mujal, R. Teodorescu, and F. Blaabjerg, "Multiresonant frequency-locked loop for grid synchronization of power converters under distorted grid conditions," *IEEE Trans. Ind. Electron*, vol. 58, no. 1, pp. 127–138, 2011.

[13] D. Dong, B. Wen, D. Boroyevich, P. Mattavelli, and Y. Xue, "Analysis of phase-locked loop low-frequency stability in three-phase grid-connected power converters considering impedance interactions," *IEEE Trans. Ind. Electron.*, vol. 62, no. 1, pp. 310–321, 2015.

[14] B. Wen, D. Boroyevich, R. Burgos, P. Mattavelli, and Z. Shen, "Analysis of DQ small-signal impedance of grid-tied inverters," *IEEE Trans. Power Electron.*, vol. 31, no. 1, pp. 675–687, 2016.

[15] X. Wang and F. Blaabjerg, "Harmonic stability in power electronic based power systems: Concept, modeling, and analysis," *IEEE Trans. Smart Grid*, 2018, in press, DOI: 10.1109/TSG.2018.2812712.

[16] I. Takahashi and T. Noguchi, "A new quick-response and high-efficiency control strategy of an induction motor," *IEEE Trans. Ind. Appl*, vol. IA-22, no. 5, pp. 820–827, 1986.

[17] M. Depenbrock, "Direct self-control (DSC) of inverter-fed induction machine," *IEEE Trans. Power Electron.*, vol. 3, no. 4, pp. 420–429, 1988.

[18] T. G. Habetler, F. Profumo, M. Pastorelli, and L. M. Tolbert, "Direct torque control of induction machines using space vector modulation," *IEEE Trans. Ind. Appl.*, vol. 28, no. 5, pp. 1045–1053, 1992.

[19] J.-K. Kang and S.-K. Sul, "New direct torque control of induction motor for minimum torque ripple and constant switching frequency," *IEEE Trans. Ind. Appl.*, vol. 35, no. 5, pp. 1076–1082, 1999.

[20] T. Noguchi, H. Tomiki, S. Kondo, and I. Takahashi, "Direct power control of PWM converter without power-source voltage sensors," *IEEE Trans. Ind. Appl.*, vol. 34, no. 3, pp. 473–479, 1998.

[21] G. Escobar, A. M. Stankovic, J. M. Carrasco, E. Galván, and R. Ortega, "Analysis and design of direct power control (DPC) for a three phase synchronous rectifier via output regulation subspaces," *IEEE Trans. Power Electron.*, vol. 18, no. 3, pp. 823–830, 2003.

[22] S. S. Lee and Y. E. Heng, "Table-based DPC for grid connected VSC under unbalanced and distorted grid voltages: Review and optimal method," *Renew. Sustain. Energy Rev.,*, vol. 76, pp. 51–61, 2017.

[23] M. Malinowski, M. Jasiński, and M. P. Kazmierkowski, "Simple direct power control of three-phase PWM rectifier using space-vector modulation (DPC-SVM)," *IEEE Trans. Ind. Electron.*, vol. 51, no. 2, pp. 447–454, 2004.

[24] D. Zhi, L. Xu, and B. W. Williams, "Improved direct power control of grid-connected DC/AC converters," *IEEE Trans. Power Electron.*, vol. 24, no. 5, pp. 1280–1292, 2009.

[25] J. Hu, L. Shang, Y. He, and Z. Zhu, "Direct active and reactive power regulation of grid-connected DC/AC converters using sliding mode control approach," *IEEE Trans. Power Electron.*, vol. 26, no. 1, pp. 210–222, 2011.

[26] Y. Gui, G. H. Lee, C. Kim, and C. C. Chung, "Direct power control of grid connected voltage source inverters using port-controlled Hamiltonian system," *Int. J. Control Autom. Syst.*, vol. 15, no. 5, pp. 2053–2062, 2017.

[27] S. Vazquez, J. I. Leon, L. G. Franquelo, J. Rodriguez, H. A. Young, A. Marquez, and P. Zanchetta, "Model predictive control: A review of its applications in power electronics," *IEEE Ind. Electron. Mag.*, vol. 8, no. 1, pp. 16–31, 2014.

[28] D.-K. Choi and K.-B. Lee, "Dynamic performance improvement of AC/DC converter using model predictive direct power control with finite control set," *IEEE Trans. Ind. Electron.*, vol. 62, no. 2, pp. 757–767, 2015.

[29] J. Hu, "Improved dead-beat predictive DPC strategy of grid-connected DC–AC converters with switching loss minimization and delay compensations," *IEEE Trans. Ind. Informat.*, vol. 9, no. 2, pp. 728–738, 2013.

[30] Y. Gui, C. Kim, and C. C. Chung, "Grid voltage modulated direct power control for grid connected voltage source inverters," in *Amer. Control Conf.*, pp. 2078–2084, 2017.

[31] Y. Gui, M. Li, J. Lu, S. Golestan, J. M. Guerrero, and J. C. Vasquez, "A voltage modulated DPC approach for three-phase PWM rectifier," *IEEE Trans. Ind. Electron.*, vol. 65, no. 10, pp. 7612–7619, Oct. 2018.

[32] Y. Gui, X. Wang, and F. Blaabjerg, "Vector current control derived from direct power control for grid-connected inverters," *IEEE Trans. Power Electron.*, pp. 1–1, 2018, in press, DOI: 10.1109/TPEL.2018.2883507.

[33] P. Kundur, N. J. Balu, and M. G. Lauby, *Power system stability and control*, vol. 7. McGraw-hill New York, 1994.

[34] F. Z. Peng and J.-S. Lai, "Generalized instantaneous reactive power theory for three-phase power systems," *IEEE Trans. Instrum. Meas.*, vol. 45, no. 1, pp. 293–297, 1996.

[35] B. K. Bose, *Power electronics and AC drives*, 1986.

[36] K. Ogata and Y. Yang, *Modern control engineering*. Prentice-Hall Englewood Cliffs, NJ, 1970.

[37] Y. Gui, C. Kim, C. C. Chung, J. M. Guerrero, Y. Guan, and J. C. Vasquez, "Improved direct power control for grid-connected voltage source converters," *IEEE Trans. Ind. Electron.*, vol. 65, no. 10, Oct. 2018.

[38] S. Buso and P. Mattavelli, *Digital control in power electronics*, vol. 5, no. 1. Morgan & Claypool Publishers, 2015.

[39] D. Holmes, T. Lipo, B. McGrath, and W. Kong, "Optimized design of stationary frame three phase AC current regulators," *IEEE Trans. Power Electron.*, vol. 24, no. 11, pp. 2417–2426, 2009.

[40] D. Pan, X. Ruan, X. Wang, H. Yu, and Z. Xing, "Analysis and design of current control schemes for LCL-type grid-connected inverter based on a general mathematical model," *IEEE Trans. Power Electron.*, vol. 32, no. 6, pp. 4395–4410, 2017.

[41] B. Wei, Y. Gui, A. Marzabal, Trujillo, J. M. Guerrero, and J. C. Vasquez, "Distributed average secondary control for modular UPS systems based microgridss," *IEEE Trans. Power Electron.*, 2018, in press, DOI:10.1109/TPEL.2018.2873793.

[42] J. Svensson, "Synchronisation methods for grid-connected voltage source converters," *IEE Proc.-Gener., Transm. Distrib.*, vol. 148, no. 3, pp. 229–235, 2001.

PLACE PHOTO HERE

Yonghao Gui (S'11-M'17) received the B.S. degree in automation from Northeastern University, Shenyang, China, in 2009, and the M.S. and Ph.D. degrees in electrical engineering from Hanyang University, Seoul, South Korea, in 2012 and 2017, respectively. From February 2017 to November 2018, he worked with the Department of Energy Technology, Aalborg University, Denmark, as a Postdoctoral Researcher. Since December 2018, he has been working with the Automation & Control Section at the Department of Electronic Systems, Aalborg University, where he is currently an Assistant Professor. He has been working with power converter control and control theory.

PLACE PHOTO HERE

Xiongfei Wang (S'10-M'13-SM'17) received the Ph.D. degree in energy technology from Aalborg University, Denmark, in 2013. He is currently a Professor and Research Program Leader for Electronic Power Grid Infrastructure at the Department of Energy Technology, Aalborg University. His current research interests include modeling and control of grid-interactive power converters, stability and power quality in power electronic based power systems. Dr. Wang serves as an Associate Editor for three IEEE journals. He received six IEEE prize paper awards and the IEEE PELS Richard M. Bass Outstanding Young Power Electronics Engineer Award in 2018.

PLACE PHOTO HERE

Frede Blaabjerg (S'86-M'88-SM'97-F'03) was with ABB-Scandia, Randers, Denmark, from 1987 to 1988. From 1988 to 1992, he got the PhD degree in Electrical Engineering at Aalborg University in 1995. He became an Assistant Professor in 1992, an Associate Professor in 1996, and a Full Professor of power electronics and drives in 1998. From 2017 he became a Villum Investigator. He is honoris causa at University Politehnica Timisoara (UPT), Romania and Tallinn Technical University (TTU) in Estonia. He has been working with power converter control the last two decades together with industry.

PLACE
PHOTO
HERE

Donghua Pan (S'12-M'15) received the B.S. and Ph.D. degrees in electrical engineering from Huazhong University of Science and Technology, Wuhan, China, in 2010 and 2015, respectively. Since September 2017, he has been with Aalborg University, Aalborg, Denmark, where he is currently a Postdoctoral Fellow with the Department of Energy Technology. His research interests include magnetic integration technique, modeling and control of grid-connected converters, and wide bandgap power conversion system. He was the recipient of the Outstanding Reviewer Award of IEEE TRANSACTIONS ON POWER ELECTRONICS in 2017 and the Best Paper Award at IEEE SPEC 2018.